CHALMERS

Chalmers Publication Library

Concurrent estimation of space and frequency variation for dielectrics: a microwave tomography system for process sensing applications

This document has been downloaded from Chalmers Publication Library (CPL). It is the author´s version of a work that was accepted for publication in:

Proceedings of the 9th International Conference on Electromagnetic Wave Interaction with Water and Moist Substances, Kansas City, MO USA, May 31 - June 3, 2011

Citation for the published paper:
Cerullo, L. ; Rylander, T. ; Gradinarsky, L. (2011) "Concurrent estimation of space and frequency variation for dielectrics: a microwave tomography system for process sensing applications". Proceedings of the 9th International Conference on Electromagnetic Wave Interaction with Water and Moist Substances, Kansas City, MO USA, May 31 - June 3, 2011 pp. 177-184.

Downloaded from: http://publications.lib.chalmers.se/publication/146203

Notice: Changes introduced as a result of publishing processes such as copy-editing and formatting may not be reflected in this document. For a definitive version of this work, please refer to the published source. Please note that access to the published version might require a subscription.

Chalmers Publication Library (CPL) offers the possibility of retrieving research publications produced at Chalmers University of Technology. It covers all types of publications: articles, dissertations, licentiate theses, masters theses, conference papers, reports etc. Since 2006 it is the official tool for Chalmers official publication statistics. To ensure that Chalmers research results are disseminated as widely as possible, an Open Access Policy has been adopted.
The CPL service is administrated and maintained by Chalmers Library.

(article starts on next page)

Concurrent estimation of space and frequency variation for dielectrics: a microwave tomography system for process sensing applications

Livia Cerullo[(1)], Thomas Rylander[(1)], Lubomir Gradinarsky[(2)], Mats Viberg[(1)], Staffan Folestad[(2)]

[(1)] Department of Signals and Systems, Chalmers University of Technology, SE-412 96 Göteborg, Sweden; Email: cerullo@chalmers.se
[(2)] AstraZeneca R&D, Pharmaceutical Development, SE-431 83 Mölndal, Sweden.

ABSTRACT

In many powder processing operations, the effective complex permittivity of the material under processing yields important information concerning the state of the process. This complex permittivity varies in general with respect to both space and frequency. For an accurate estimation of the process material parameters, it is important to be able to incorporate these dependencies in the estimation algorithm. Here, we present a rather general type of parameterization that is tailored for this type of situation. The parameterization is described in terms of a parameterization mesh, which makes it feasible to refine the computational mesh without influencing the number of degrees of freedom in the estimation problem. A test case demonstrates that our approach can yield accurate reconstructions.

Keywords: Microwave process tomography, dispersive material, reconstruction algorithm

1 INTRODUCTION

The processing industries, in particular where manufacturing comprise powder processing operations, will benefit from access to advanced sensor technologies for in-situ measurements. Of special interest are techniques enabling measurements of solid material movements and/or transport in real time. Novel routes here go beyond measuring in one dimension. Use of sensor arrays enables 2 and 3 dimensional parameter measurements and opens unique opportunities for advanced process monitoring and control, i.e., process tomography [1],[2]. So far a few sensor techniques have been used in process tomography, e.g., Electrical Capacitance (ECT) [1],[3]. Here, the conventional techniques for process tomography are extended and a novel application of microwave sensing, i.e., Microwave Process Tomography (MPT) is introduced. Compared to existing techniques, MPT is very competitive and provides relatively high resolution images in a non-destructive and non-invasive manner, when contrasted to low frequency or static tomographic systems such as ECT. Microwave tomography have been thoroughly investigated over the last two decades mainly for medical applications [4],[5],[6]. In the last few years, it has started expanding as monitor for industrial processes. In this direction, in fact, the wood industry developed microwave imaging systems for imaging of buried objects in wood trunks [7] and for observing defects in wood slabs [8]. Furthermore, the gas-oil industry developed an experimental system for the imaging of multiphase flows [9].

In this paper, we present a 2D model of a microwave tomography system for the monitoring of powder processes. The inverse algorithm is tested for the estimation of the complex permittivity associated with a material that is part of a process, where the space and frequency variation of the complex permittivity is estimated concurrently. We consider a test geometry that consists of a circular cylindrical cavity equipped with N_{p} parallel-plate waveguide sensors, where the electric field is parallel to the cylinder axis. The continuum form of Maxwell's equations is solved by means of the finite element method (FEM) [10]. The reconstruction algorithm is formulated as a minimization problem with a

goal function that involves the misfit between the computed and the measured scattering parameters, where we average the absolute value of the misfit over a frequency range and the number of waveguide sensors. The first order variation of the goal function is evaluated exploiting the sensitivity of the scattering parameters with respect to changes in the material parameters [2]. We formulate the sensitivity in terms of the solution of (i) the original scattering problem and (ii) the solution of an adjoint problem. The unknown complex permittivity is represented on a parameterization mesh, where it is parameterized by means of a set of space dependent basis functions with frequency dependent coefficients. Here, the coefficients involve unknown parameters that are determined in the reconstruction problem. An advantage with this construction is that the parameterization and its number of degrees of freedom are independent of the computational mesh.

2 MODEL

The 2 dimensional model of the microwave tomography system is shown in Fig. 1. It consists of a circular cylindrical cavity of radius r_{c} equipped with N_{p} parallel-plate waveguide sensors, uniformly located around the cavity perimeter. The waveguide dimensions are chosen such that higher-order modes are negligible at the waveguide ports. The reconstruction region is located inside the cavity $x^2 + y^2 \leq r_{\mathrm{c}}^2$.

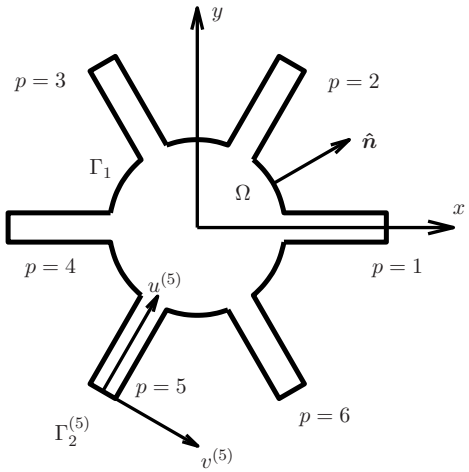

Fig. 1: *Geometry of the microwave tomography system. The* $(u^{(5)}, v^{(5)})$ *local coordinate system is adopted for the Robin boundary condition at* $\Gamma_2^{(5)}$ *associated with port* $p = 5$.

For this geometry, we seek the magnetic field that satisfies the vector Helmholtz equation

$$\nabla \times (\epsilon_{\mathrm{c}}^{-1} \nabla \times \boldsymbol{H}) - \omega^2 \mu_0 \boldsymbol{H} = \boldsymbol{0} \tag{1}$$

on the domain Ω. Here, the magnetic field $\boldsymbol{H}$ is transverse to the cylinder axis of the cavity and ϵ_{c} is the complex permittivity in the region subject to reconstruction. At the waveguide ports $\Gamma_2^{(p)}$, we exploit the Robin boundary condition

$$\hat{\boldsymbol{n}} \times (\epsilon_{\mathrm{c}}^{-1} \nabla \times \boldsymbol{H}) + j\omega Z_{10}\, \hat{\boldsymbol{n}} \times (\hat{\boldsymbol{n}} \times \boldsymbol{H}) = 2j\omega Z_{10} \hat{\boldsymbol{n}} \times \hat{\boldsymbol{n}} \times \boldsymbol{H}_p^+. \tag{2}$$

Here, Z_{10} is the wave impedance, $\hat{\boldsymbol{n}}$ is the outward pointing normal and $\boldsymbol{H}_p^+$ is the incident field at port p, represented by the fundamental waveguide mode. For the PEC boundary Γ_1, we use the Neumann

boundary condition

$$\hat{\boldsymbol{n}} \times (\epsilon_{\mathrm{c}}^{-1} \nabla \times \boldsymbol{H}) = \boldsymbol{0}. \tag{3}$$

The finite element method (FEM) is exploited to solve this boundary value problem, where the magnetic field is expanded in terms of edge elements [10]. The weak formulation [10] for this problem is expressed as

$$a(\boldsymbol{w}, \boldsymbol{H}) = b(\boldsymbol{w}) \tag{4}$$

where

$$\begin{aligned} a(\boldsymbol{w}, \boldsymbol{H}) = & \int_{\Omega} [\epsilon_{\mathrm{c}}^{-1} (\nabla \times \boldsymbol{w}) \cdot (\nabla \times \boldsymbol{H}) - \omega^2 \mu_0 \, \boldsymbol{w} \cdot \boldsymbol{H}] d\Omega \\ & + \sum_{p=1}^{N_{\mathrm{p}}} \gamma^{(p)} \int_{\Gamma_2^{(p)}} (\hat{\boldsymbol{n}} \times \boldsymbol{w}) \cdot (\hat{\boldsymbol{n}} \times \boldsymbol{H}) d\Gamma \end{aligned} \tag{5}$$

$$b(\boldsymbol{w}) = \sum_{p=1}^{N_{\mathrm{p}}} b_p(\boldsymbol{w}) = - \sum_{p=1}^{N_{\mathrm{p}}} \int_{\Gamma_2^{(p)}} \boldsymbol{w} \cdot \boldsymbol{Q}^{(p)} \, d\Gamma \tag{6}$$

with $\boldsymbol{w}$ being the set of test functions chosen accordingly to the Galerkin's method [10]. Here, $\gamma^{(p)} = j\omega Z_{10}$ and $\boldsymbol{Q}^{(p)} = 2j\omega Z_{10} \hat{\boldsymbol{n}} \times \hat{\boldsymbol{n}} \times \boldsymbol{H}_p^+$.

3 RECONSTRUCTION ALGORITHM

The reconstruction algorithm exploits the sparse nonlinear solver (SNOPT) that is part of TOMLAB [11]. The SNOPT solver is based on the sequential quadratic programming (SPQ) and it allows to solve large scale nonlinear problems subject to linear and/or nonlinear constraints.
Given the measured scattering parameters S_{pq}^{M}, the complex permittivity $\epsilon_{\mathrm{c}}(\boldsymbol{r}, \omega; \boldsymbol{d})$ in the interior of the cavity is reconstructed by minimizing the goal function

$$g(\boldsymbol{d}) = \left[\frac{1}{N_{\mathrm{p}}^2} \sum_{p=1}^{N_{\mathrm{p}}} \sum_{q=1}^{N_{\mathrm{p}}} \frac{1}{f_{\mathrm{U}} - f_{\mathrm{L}}} \int_{f_{\mathrm{L}}}^{f_{\mathrm{U}}} |S_{pq}^{\mathrm{C}}(f; \boldsymbol{d}) - S_{pq}^{\mathrm{M}}(f)|^2 df \right]^{\frac{1}{2}}, \tag{7}$$

In (7), S_{pq} are the scattering parameters, $S_{pq} = V_{0p}^- / V_{0q}^+$, with V_{0p}^- being the reflected voltage amplitude at port p and V_{0q}^+ the incident at port p. Since the voltages are proportional to the field amplitudes $E_{0p}^{\pm}$, with a constant proportionality for all ports, the scattering parameters reduce to

$$S_{pq} = \frac{E_{0p}^-}{E_{0q}^+} = \frac{E_{0p}^+}{E_{0q}^+} e^{-2jk_v v^{(p)}} - \frac{\mu_0}{jk_v w_{\mathrm{w}} E_{0p}^+ E_{0q}^+} b_p(\boldsymbol{H}), \tag{8}$$

where $k_v = \sqrt{(\omega/c_0)^2 - (\pi/w_{\mathrm{w}})^2}$ denotes the wave number, w_{w} the waveguide width and $c_0 = 1/\sqrt{\epsilon_0 \mu_0}$ the speed of light.
The first order variation δS_{pq} of the scattering parameters S_{pq} with respect to a perturbation $\delta\epsilon_{\mathrm{c}}$ in the permittivity ϵ_{c} is computed by means of (i) the solution of the original problem $\boldsymbol{H}_{\mathrm{orig}}$ and (ii) the solution of an adjoint problem $\boldsymbol{H}_{\mathrm{adj}}$. Due to the reciprocity of Maxwell's equations, the original field

problem and the adjoint field problem are identical for the situation considered in this article. Thus, the first order variation δS_{pq} is given by [2]

$$\delta S_{pq} = -\frac{\mu_0}{jk_v w_{\mathrm{w}} E^+_{p,\mathrm{adj}} E^+_{q,\mathrm{orig}}} \int_\Omega \frac{\delta\epsilon_{\mathrm{c}}}{\epsilon_{\mathrm{c}}^2} (\nabla \times \boldsymbol{H}_{\mathrm{adj}}) \cdot (\nabla \times \boldsymbol{H}_{\mathrm{orig}}) d\Omega \tag{9}$$

where $E^+_{q,\mathrm{orig}}$ is the incident field amplitude when port q is excited, $E^+_{p,\mathrm{adj}}$ the incident field amplitude when port p is excited. Equation (9) is used to evaluate the first order variation of the goal function $g(\boldsymbol{d})$ with respect to a perturbation $\delta\epsilon_{\mathrm{c}}$. This yields an efficient optimization procedure in the sense that the computational cost for the gradient is independent of the number of degrees of freedom in the optimization problem.

3.1 Parameterization

For inverse problems, it is common to associate one material parameter value to each element of the computational mesh, see e.g. [4],[12]. For a method that exploits a linear approximation of the solution, the total number of degrees of freedom is very large and it increases dramatically as the mesh is refined. As a consequence, the inverse problem tends to become ill-conditioned and the optimization algorithm may get stuck in local minima, where such problems may be mitigated by regularization [13].

Here, we introduce a parameterization mesh that is used for the representation of the material parameter. The spatial variation of the complex permittivity is parameterized in terms of basis functions $\varphi_k(\boldsymbol{r})$, where each basis function is multiplied by a coefficient $a_k(\omega; \boldsymbol{d}_k)$. Furthermore, the coefficients $a_k(\omega; \boldsymbol{d}_k)$ are frequency dependent and, in addition, they depend on a set of parameters $\boldsymbol{d}_k$ that influence the frequency response of the material. Consequently, the complex permittivity is defined as

$$\epsilon_{\mathrm{c}}(\boldsymbol{r}, \omega; \boldsymbol{d}) = \epsilon_0 \sum_{k=1}^{K} a_k(\omega; \boldsymbol{d}_k) \varphi_k(\boldsymbol{r}). \tag{10}$$

where the vacuum permittivity is denoted ϵ_0. Here, $\boldsymbol{d}$ is a global parameter vector that consists of the local parameters $\boldsymbol{d}_k$ associated with the k-th basis function, i.e. $\boldsymbol{d} = [\boldsymbol{d}_1, \boldsymbol{d}_2, \ldots, \boldsymbol{d}_K]$. It should be noted that this representation allows for both a continuous and discontinuous permittivity.

3.1.1 Spatial variation

There is a large flexibility for the choice of the set of basis functions. In a previous article [2], the authors exploited the global Bézier polynomials to describe the radial variation of an axisymmetric material distribution, where the global basis functions avoid the necessity of creating a parameterization mesh. The Bézier polynomials are useful in the sense that they guarantee that the interpolated function resides in the convex hull of the control points. Here, we wish to treat more general cases, where the material distribution is not necessarily axisymmetric. Thus, we use Lagrangian polynomials [10] defined on the parameterization mesh that consists of triangular elements, where the size of these elements is fixed as the computational mesh is refined. Fig. 2 shows the geometry together with an example of a parameterization mesh. Here, the region subject to reconstruction is located inside the circular cavity defined by $x^2 + y^2 \leq r_{\mathrm{c}}^2$ as shown in Fig. 1. Given that the parameterization mesh consists of triangles with straight edges, there are sliver shaped regions outside the gray area shown in Fig. 2 but inside the region $x^2 + y^2 \leq r_{\mathrm{c}}^2$. In these slivers, we extend the basis functions $\varphi_k(\boldsymbol{r})$ for the triangle that shares an edge with the sliver, i.e. we evaluate the standard expressions for the

basis functions $\varphi_k(\boldsymbol{r})$ despite the fact that a point inside the sliver is slightly outside the domain of the triangle.

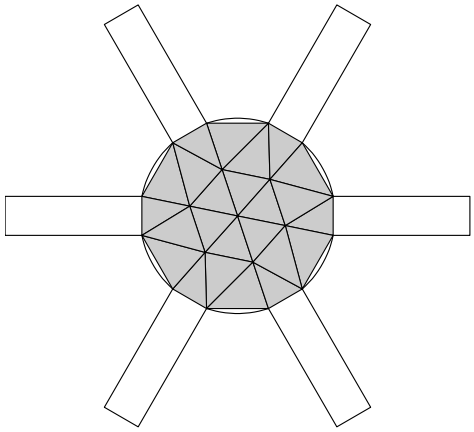

Fig. 2: *Geometry of the microwave tomography system together with the parameterization mesh, which is shown by the gray triangles.*

Typically, we would use piecewise constant, linear or quadratic basis functions. Here, the piecewise constant basis functions yield a material distribution that is discontinuous with respect to space. For the linear and quadratic Lagrangian basis functions, we can choose to enforce continuity at the edges between the elements of the parameterization mesh by means of linear constraints provided to TOMLAB. As a special case, we may also treat the more conventional approaches [4],[12] if we make the parameterization mesh identical to the computational mesh and exploit piecewise constant constant basis functions.

3.1.2 Frequency variation

Microcrystalline cellulose (MCC) is a commonly used pharmaceutical material. Reference [14] shows that the MCC exhibits dispersive behavior in the microwave region due to the absorbed water. Its permittivity is primarily dependent on its moisture content and the measured material amount or bulk density [15]. In-line single point measurements of MCC moisture has been demonstrated previously [15]. Therefore, it is important to allow for a variety of dispersion models in the estimation procedure.
For testing purposes, we consider a lossy material with $\epsilon_{\mathrm{c}}(\boldsymbol{r},\omega) = \epsilon_0\epsilon_{\mathrm{r}}(\boldsymbol{r}) - j\sigma(\boldsymbol{r})/\omega$ and, thus, we use the coefficients

$$a_k(\omega;\boldsymbol{d}_k) = d_{k,1} + \frac{d_{k,2}}{j\omega\epsilon_0}. \tag{11}$$

Here, $d_{k,1}$ represents the relative permittivity ϵ_{r} associated with the k-th basis function and, correspondingly, $d_{k,2}$ represents the conductivity σ. For the k-th basis function, we have the parameters $\boldsymbol{d}_k = [d_{k,1}, d_{k,2}]$. In the same fashion, other dispersive material models can be accounted for such as the Debye, Lorentz or the Cole-Cole material model.

4 NUMERICAL TESTS

We test this algorithm for a simple test case, where we wish to reconstruct a material distribution with the complex permittivity $\epsilon_{\mathrm{c}}(\boldsymbol{r},\omega) = \epsilon_0\epsilon_{\mathrm{r}}(\boldsymbol{r}) - j\sigma(\boldsymbol{r})/\omega$. The concurrent estimation of the complex

permittivity is carried out for the geometry shown in Fig. 1. It consists of a cavity with radius $r_{\mathrm{c}} = 0.1$ m, six waveguide sensors ($N_{\mathrm{p}} = 6$) of width $w_{\mathrm{w}} = 0.04$ m and length $l_{\mathrm{w}} = 0.14$ m. The reconstruction is performed using six discrete frequencies that are uniformly distributed in the interval from $f_{\mathrm{L}} = 3.8$ GHz to $f_{\mathrm{U}} = 4.2$ GHz. For the reconstruction, the resolution for the FEM mesh is set to 20 points per wavelength.

Fig. 3 shows a parameterization mesh that is composed of 24 elements. Given that we use the coefficients in (11) together with piecewise constant basis functions, we have a total of 48 degrees of freedom in the reconstruction problem. The gray triangular elements in the parameterization mesh shown in Fig. 3 are characterized by $\epsilon_{\mathrm{r}} = 1$ and $\sigma = 0$, i.e. air. The triangular element indicated by the black color has the material parameters $\epsilon_{\mathrm{r}} = 1.5$ and $\sigma = 0.02$. We perform a sequence of FEM computations with an increasing number of points per wavelength, where the computational mesh is refined hierarchically. In particular, the number of points per wavelength is $\lambda/h = 5, 10, 15, 20, 30, 45, 60$ where h is the cell size of the computational mesh and λ is the free-space wavelength for the highest frequency f_{U}. We extrapolate the computed scattering matrices to zero cell size and use this result as an artificially generated S_{pq}^{M} for testing purposes.

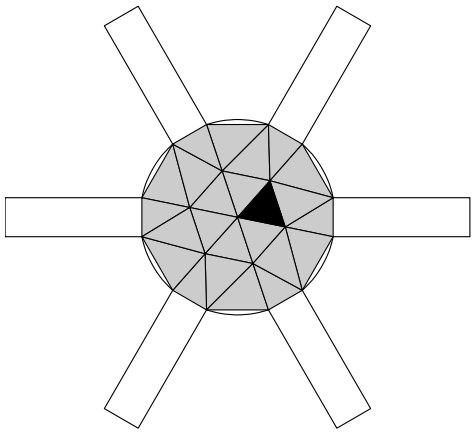

Fig. 3: *Geometry of the microwave tomography system together with the parameterization mesh:* $\epsilon_{\mathrm{r}} = 1.5$ *and* $\sigma = 0.02$ *for the triangular element shown by the black color; and* $\epsilon_{\mathrm{r}} = 1$ *and* $\sigma = 0$ *for the triangular elements shown by the gray color.*

We initiate the reconstruction algorithm with $d_{k,1} = 1$ and $d_{k,2} = 0$ for $k = 1, \ldots, 24$. The optimization algorithm that attempts to minimize the misfit $|S_{pq}^{\mathrm{C}}(f; \boldsymbol{d}) - S_{pq}^{\mathrm{M}}(f)|$ evolves the parameters $d_{k,1}$ and $d_{k,2}$ in an iterative manner such that the misfit is reduced, when subject to the constraints $1 \leq d_{k,1} \leq 5$ and $0 \leq d_{k,2} \leq 0.8$. The evolution of the relative permittivity $d_{k,1}$ for each element k is shown in Fig. 4(a) and the corresponding result for the conductivity $d_{k,2}$ is shown in Fig. 4(b): thick curve – value for the black element in Fig. 3; and thin curves – values for the gray elements in Fig. 3. Furthermore, the material distribution at the end of the reconstruction procedure is shown in Fig. 5: (a) the reconstructed relative permittivity; and (b) the reconstructed conductivity.

The iterative reconstruction algorithm has converged within 60 iterations to the values $d_{k,1} = 1.46$ and $d_{k,2} = 0.019$ for the black element in Fig. 3. For the gray elements in Fig. 3, we find that $d_{k,1} = 1$ and $0 \leq d_{k,2} < 8 \cdot 10^{-4}$. We also tested the algorithm with the initial values $d_{k,1} = 1.5$ and $d_{k,2} = 0.02$ for the black element in Fig. 3, whereas we set $d_{k,1} = 1$ and $d_{k,2} = 0$ for all the other elements

in the parameterization mesh. Clearly, this is the correct parameter vector and, again, it converges to the same values as for the case where the initial material distribution is $\epsilon_{\mathrm{r}} = 1$ and $\sigma = 0$. The difference between the correct values and the estimated values is attributed to the fact that the field solver exploited for the reconstruction algorithm uses about 20 points per wavelength, whereas the the extrapolated value is used for S_{pq}^{M} in order to avoid the inverse crime.

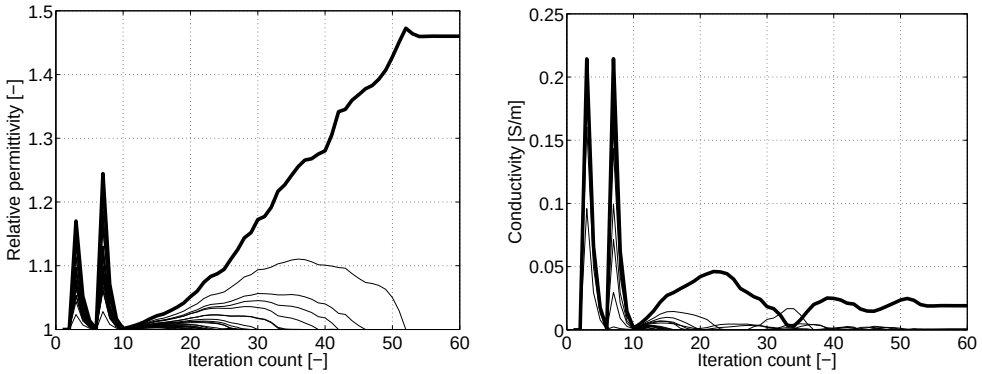

(a) (b)

Fig. 4: *Evolution of (a) the relative permittivity $d_{k,1}$ and (b) the conductivity $d_{k,2}$: thick curve – black element in Fig. 3; and thin curves – gray elements in Fig. 3.*

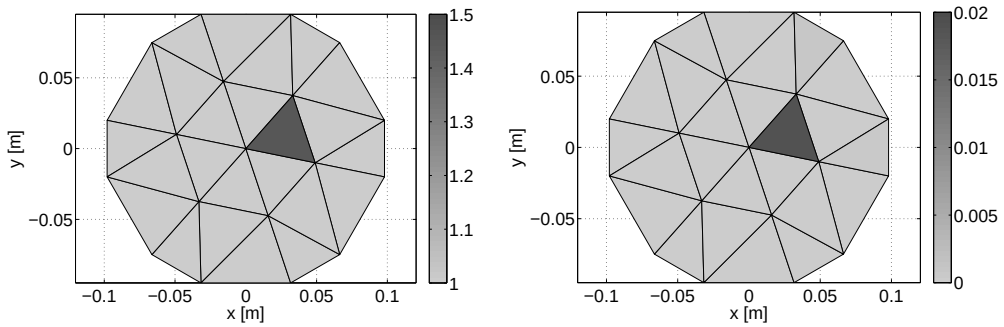

(a) (b)

Fig. 5: *Reconstruction of (a) the relative permittivity and (b) the conductivity.*

5 CONCLUSIONS

Given a microwave tomography system or similar measurement system, we have presented a technique that allows for the representation of a rather general complex permittivity that is both inhomogeneous and exhibits dispersive properties. It exploits a parameterization mesh and a set of basis functions represented on this mesh. The material parameter subject to reconstruction is expanded in terms of the space dependent basis functions associated with the parameterization mesh, where each basis function is multiplied by a frequency dependent coefficient. The coefficients also involve the parameters to be estimated and, thus, it is feasible to model e.g. Debye, Lorentz or Cole-Cole media.

The parameterization mesh can consist of triangles or quadrilaterals for 2 dimensional problems. Our approach is easily extended to 3 dimensional problems where the parameterization mesh can consist

of tetrahedrons, prisms and hexahedrons. Thus, it is possible to use this type of representation for quite arbitrary domains. Moreover, the cell size for the computational mesh (used to represent the field solution) is disconnected from the parameterization mesh. This is advantageous since it allows for mesh refinement in order to achieve more accurately computed scattering parameters and their sensitivities without increasing the number of degrees of freedom that are used to describe the material parameter. Initial tests demonstrate that for an estimation problem with 48 degrees of freedom, the reconstruction algorithm converges within 60 iterations.

REFERENCES

[1] H. Wang, P. Senior, R. Mann, and W. Q. Yang, "Online solids moisture measurement and optimum control of fluidised bed dryer," *Chemical Engineering Science*, no. 64, pp. 2893–2902, 2009.

[2] L. Cerullo, T. Rylander, and M. Viberg, "Determination of model order for inverse scattering applications," in *Proceedings of the V European Conference on Computational Fluid Dynamics ECCOMAS CFD 2010 J. C. F. Pereira, A. Sequeira and J. M. C. Pereira (Eds) Lisbon, Portugal,14-17 June 2010*, 2010.

[3] H. Wang, L. Gradinarsky, S. Folestad, and L. Cerullo, "Imaging pharmaceutical multi-processes in fluidized bed by electrical capacitance tomography," in *AIChE Annual Meeting; 07 Nov 2010-12 Nov 2010; Salt Lake City, Utah, USA. AIChE*, 2010.

[4] A. Fhager and M. Persson, "Using a priori data to improve the reconstruction of small objects in microwave tomography," *Microwave Theory and Techniques, IEEE Transactions on*, vol. 55, no. 11, 2007.

[5] M. Hawley, A. Broquetas, L. Jofre, J. Bolomey, and G. Gaboriaud, "Microwave imaging of tissue blood content changes," *J. Biomed. Eng*, vol. 13, 1991.

[6] S. Semenov, R. Svenson, A. Bulyshev, A. Souvorov, A. Nazarov, Y. Sizov, V. Posukh, A. Pavlovsky, P. Repin, and G. Tatsis, "Spatial resolution of microwave tomography for detection of myocardial ischemia and infarction-experimental study on two-dimensional models," *Microwave Theory and Techniques, IEEE Transactions on*, vol. 48, no. 4, 2000.

[7] A. Salvade, M. Pastorino, R. Monleone, A. Randazzo, T. Bartesaghi, G. Bozza, and S. Poretti, "Microwave imaging of foreign bodies inside wood trunks," in *Imaging Systems and Techniques, 2008. IST 2008. IEEE International Workshop on*, pp. 88–93, 2008.

[8] M. Pastorino, A. Salvade, R. Monleone, T. Bartesaghi, G. Bozza, and A. Randazzo, "Detection of defects in wood slabs by using a microwave technique," in *Instrumentation and Measurement Technology Conference Proceedings, 2007. IMTC 2007. IEEE*, 2007.

[9] Z. Wu, H. McCann, L. Davis, J. Hu, A. Fontes, and C. G. Xie, "Microwave-tomographic system for oil- and gas-multiphase-flow imaging," *Meas. Sci. Technol.*, vol. 20, 2009.

[10] J. Jin, *The Finite Element Method in Electromagnetics*. John Wiley & Sons, Inc, 2nd ed., 2002.

[11] K. Holmström, A. O. Göran, and M. M. Edvall, *User's guide for Tomlab 7*. Tomlab Optimization AB, Västerås Technology Park, Trefasgatan 4, SE-72130 Västerås, Sweden, 2009.

[12] E. Wadbro and M. Berggren, "High contrast microwave tomography using topology optimization techniques," *J. Comput. Appl. Math.*, vol. 234, pp. 1773–1780, 2010.

[13] T. Isernia, V. Pascazio, and R. Pierri, "On the local minima in a tomographic imaging technique," *IEEE transaction on geoscience and remote sensing*, vol. 39, no. 7, 2001.

[14] M. Kent and W. Meyer, "Dielectric relaxation of absorbed water in microcrystalline cellulose," *J. Phys. D: Appl. Phys.*, vol. 16, pp. 915–925, 1983.

[15] L. Gradinarsky, H. Brage, B. Lagerholm, I. Niklasson, B. Folestad, and S. Folestad, "In situ monitoring and control of moisture content in pharmaceutical powder processes using an open-ended coaxial probe," *Meas. Sci. Technol.*, vol. 17, pp. 1847–1853, 2006.